

La-dilution effects in antiferromagnetic TbRhIn₅ single crystals

R. Lora-Serrano,¹ D. J. Garcia,^{1,2} E. Miranda,¹ C. Adriano,¹ C. Giles,¹ J. G. S. Duque,¹ and P. G. Pagliuso¹

¹*Instituto de Física “Gleb Wataghin,” UNICAMP, 13083-970 Campinas, São Paulo, Brazil*

²*Centro Atómico Bariloche, Comisión Nacional de Energía Atómica, 8400 S.C. de Bariloche, Argentina*

(Received 29 July 2008; revised manuscript received 11 November 2008; published 21 January 2009)

We report on measurements of temperature-dependent magnetic susceptibility, resonant x-ray magnetic scattering (XRMS), and heat capacity on single crystals of Tb_{1-x}La_xRhIn₅ for nominal concentrations in the range $0 \leq x < 1$. TbRhIn₅ is an antiferromagnetic (AFM) compound with $T_N \approx 46$ K, which are the highest T_N values along the RRhIn₅ series (R : rare earth). We explore the suppression of the AFM state as a function of La doping considering the effects of La-induced dilution and perturbations to the tetragonal crystalline electrical field on the long-range magnetic interaction between the Tb³⁺ ions. Additionally, we also discuss the role of disorder. Our results and analysis are compared to the properties of the nondoped compound and of other members of the RRhIn₅ family and structurally related compounds (R_2 RhIn₈ and RIn₃). The XRMS measurements reveal that the commensurate magnetic structure with the magnetic wave vector $(0\frac{1}{2}\frac{1}{2})$ observed for the nondoped compound is robust against doping perturbations in Tb_{0.6}La_{0.4}RhIn₅ compound.

DOI: [10.1103/PhysRevB.79.024422](https://doi.org/10.1103/PhysRevB.79.024422)

PACS number(s): 75.50.Ee, 75.10.Dg, 75.25.+z, 75.30.Kz

I. INTRODUCTION

The magnetic dilution and percolation problems are directly connected to each other and continue to be attractive subjects in the field of magnetism and strongly correlated electrons systems (SCES). This is because different and interesting ground states (GS) can be generally tuned by chemical substitution in these systems. In particular, for heavy-fermion compounds, chemical substitution is a very important tuning parameter as it may strongly affect the interplay between the intrasite Kondo effect and the intersite long-range Ruderman-Kittel-Kasuya-Yoshida (RKKY) magnetic interaction, driving the system from a magnetic ordered state [for instance, antiferromagnetic (AFM) to a nonmagnetic heavy-electron paramagnetic metal].¹ Interestingly, in the vicinity of the magnetic phase, unconventional superconductivity (USC) and non-Fermi-liquid (NFL) behavior may be found in many cases. In terms of dilution at the heavy-fermion ion site, a nonobvious evolution from a magnetic or nonmagnetic dense Kondo lattice state to a Kondo single-impurity regime in the very diluted regime is expected.¹

The family of heavy fermions Ce_mM_nIn_{3m+2n} ($M = \text{Co, Rh, Ir}$; $m = 1$ and 2 ; and $n = 1$) have been proving to be a great series to explore the role of doping in tuning a variety of ground states such as AFM, USC, NFL behavior, and Fermi liquid (FL) behavior in high-quality single crystals. All these interesting GSs have been found in these systems in specific regions of their rich phase diagrams.²⁻⁸

Dilution studies⁹⁻¹⁷ in the above series were performed for both ambient pressure AFM (CeRhIn₅) and USC (CeCoIn₅) heavy-fermion compounds. In terms of suppression of AFM, a critical La concentration of about $x_c = 0.40$ was obtained from the extrapolation of dT_N/dx slope to $T \rightarrow 0$ for La-doped Ce_{1-x}La_xRhIn₅.⁹ This is consistent with the theoretical percolation threshold for a two-dimensional (2D)-spin system.¹⁸ On the other hand, measurements of thermal expansion and magnetostriction in Ce_{0.60}La_{0.40}RhIn₅ single crystals¹⁰ suggested the evolution of the crystalline electrical-field (CEF) ground state as a function of La con-

centration and revealed the presence of remaining anisotropic short-range magnetic correlations, which was consistent with earlier reported heat-capacity data.^{9,11} In terms of La-doping-induced changes in the electronic structure, recent de Haas-van Alphen (dHvA) measurements in Ce_{1-x}La_xRhIn₅ has shown a near insensitivity of the Fermi-surface topology to x implying almost entirely localized f -electron behavior.¹² The magnetic structure of the CeRhIn₅ is also nearly unaffected by 10% of La substitution.¹⁴ In addition, Paglione *et al.*¹⁹ recently substituted Ce³⁺ ion by magnetic and nonmagnetic R^{3+} ions to study the T -linear behavior of resistivity in Ce_{1-x}R_xCoIn₅. They have demonstrated that both superconducting critical temperature T_c and Kondo lattice coherence temperature T_{coh} are insensitive to the magnetic configuration of the R ion, evidencing the separation between the physics behind the Kondo lattice and the non-Fermi-liquid transport behavior in CeCoIn₅.

More recently, studies of Ce_{0.90}La_{0.10}RhIn₅ under pressure have revealed that the La doping shifts the pressure-induced superconducting phase to higher pressures, indicating that the main effect of the La doping in CeRhIn₅ in this range of La concentration is the decreasing of the Kondo coupling.²⁰

Regarding the effect of La dilution in the properties of the superconducting and dense Kondo lattice CeCoIn₅, the pair breaking by nonmagnetic La results in a depression of T_c that extrapolates to zero for a critical La concentration $x_c \approx 0.18$ indicating a strong gap anisotropy.¹⁶ Further, thermal-conductivity and specific-heat experiments at low temperature revealed that the suppression of T_c is followed by the increase in the residual electronic specific heat but along with the decrease in the residual electronic thermal conductivity. This contrasting result suggests a coexistence between unpaired electrons and nodal quasiparticles.¹⁵ Still, in the Ce_{1-x}La_xCoIn₅ series, an interesting evolution of the normal-state properties was also verified through the finding of scaling laws for the specific-heat and magnetic-susceptibility data suggesting two separated energy scales: one from a single-impurity Kondo temperature T_K and the other from a larger intersite spin-liquid temperature T^* which involves the intersite antiferromagnetic correlations.¹⁷ From their high- T

heat-capacity data, they claimed that the CEF scheme remains unchanged as a function of La concentration.¹⁷

However, achieving a complete microscopic understanding of the evolution of physical properties induced by La doping in CeRhIn₅ and CeCoIn₅ is a very difficult task as the doping may affect simultaneously, and in a combined way, the in-site Kondo effect, the intersite RKKY interaction, the CEF effects, the electronic structure, and also introducing disorder. In this sense, the study of structurally related compounds within the $R_mM_n\text{In}_{3m+2n}$ family has been successfully used to understand the evolution of 4*f*-electron magnetism for many members of the series in situations where some of the contributions above can be negligible.^{21–28} For instance, in the $\text{Gd}_mM_n\text{In}_{3m+2n}$ ($M=\text{Rh}$ and Ir) compounds, as Gd^{3+} is a pure ($S=7/2, L=0$) spin ion, the RKKY interaction and its dependence with electronic structure is the main contribution.^{22–24} For the Nd- and Tb-based members of the $R_mM_n\text{In}_{3m+2n}$ family,^{21,25,26,28,29} both RKKY interaction and CEF effects are present, and the CEF contribution can be evaluated for Krammers ($\text{Nd}^{3+}, J=9/2$) and non-Krammers ions ($\text{Tb}^{3+}, J=6$) without the complexity of the Kondo lattice behavior of the Ce-based compounds.

In this work, we have systematically studied dilution effects on TbRhIn₅, which is an isostructural magnetic relative of CeMIn₅, as the Tb^{3+} ions are substituted by nonmagnetic La^{3+} ions for $0 \leq x < 1$. The TbRhIn₅ intermetallic compound²⁶ orders antiferromagnetically with a commensurate magnetic structure ($0\frac{1}{2}\frac{1}{2}$) below $T_N \sim 46$ K, which is the highest T_N among the $RR\text{In}_5$ compounds. Results from magnetic-susceptibility and specific-heat data taken below ~ 150 K down to 2 K in $\text{Tb}_{1-x}\text{La}_x\text{RhIn}_5$ ($x=0.15, 0.40$, and 0.50) as well as the magnetic structure determination for the $\text{Tb}_{0.60}\text{La}_{0.40}\text{RhIn}_5$ compound using resonant XRMS are reported. From the analysis of the evolution of magnetic properties of the studied samples as a function of La concentration, we evaluate the role of the different mechanisms for the suppression of the long-range AFM coupling by considering dilution, changes in the CEF scheme, and the introduction of disorder. Additionally, the XRMS measurements have shown that the commensurate magnetic structure ($0\frac{1}{2}\frac{1}{2}$) observed for the nondoped compound is robust against doping perturbations, indicating that no changes in the relative spin interaction of neighboring Tb spins are taking place. These results are discussed in a broader prospective considering other members of the $R_mM_n\text{In}_{3m+2n}$ family.

II. EXPERIMENTAL

All measurements were taken on single-crystalline samples grown by the indium excess flux.³⁰ Typical crystal sizes were $0.5 \text{ cm} \times 0.5 \text{ cm} \times \text{few mm}$. The tetragonal HoCoGa₅-type structure and crystals phase purity were confirmed at ambient temperature by x-ray powder diffraction. Magnetization measurements were performed as a function of temperature in a commercial superconducting quantum interference device (SQUID) magnetometer. Specific-heat data were taken using a commercial physical property measurement system (PPMS) using the adiabatic relaxation method in the temperature range between 1.9 and 150 K. The

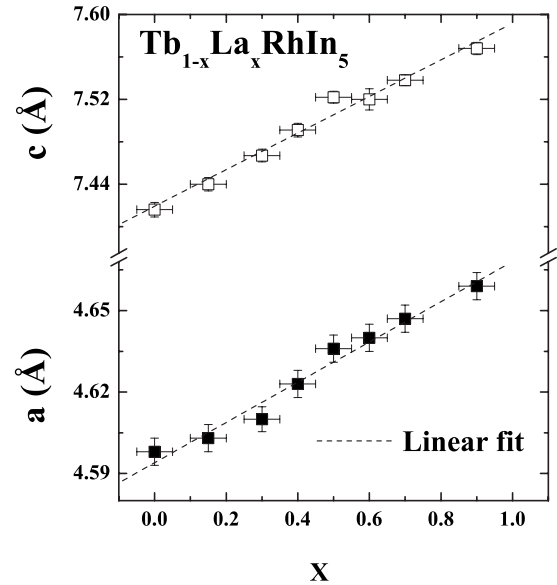


FIG. 1. Lattice cell parameters a and c vs lanthanum concentration x for the $\text{Tb}_{1-x}\text{La}_x\text{RhIn}_5$ system. The dotted line is a linear fit to both data sets.

resonant XRMS experiments were performed at the XRD2 beamline of the Laboratório Nacional de Luz Síncrotron (LNLS) in Campinas, Brazil, and the description of the experimental setup used can be found in Refs. 23, 26, and 31.

III. RESULTS AND DISCUSSION

Figure 1 displays the cell parameters for $x=0, 0.15, 0.30, 0.40, 0.50, 0.60, 0.70$, and 0.90 lanthanum concentrations. Both parameters expand linearly with x (taking x as the nominal value given by the Ce/La ratio in the starting materials) as the smaller Tb^{3+} ion is substituted into the $1a$ crystallographic site by larger La^{3+} ion, in agreement with the Vegard's law. The cell parameters a and c were determined from least-squares fits of the Bragg-peak positions (2θ) in the x-ray powder-diffraction patterns.³²

Figure 2 shows the magnetic-susceptibility $\chi(T)$ and heat-capacity $C(T)/T$ data for representative samples of the $\text{Tb}_{1-x}\text{La}_x\text{RhIn}_5$ series. $\chi(T)$ data [Figs. 2(a)–2(c)] were taken at a magnetic field $H=1$ kOe applied parallel to the $[100]$ crystallographic direction (χ_{\perp}) and along the c axis ($[001]$ direction) (χ_{\parallel}). Figures 2(d)–2(f) display the temperature dependence of the magnetic specific heat per Tb mole. The phonon contribution to the total specific heat was subtracted using the data of nonmagnetic YRhIn₅. The solid curves in Fig. 2 are the best fits to the data using the mean-field (MF) model of Ref. 28 which includes an isotropic exchange between rare-earth ions and the tetragonal crystal-field terms into the Hamiltonian.

The actual La concentration in our samples was estimated from linear fits to the inverse of the magnetic susceptibility at high T ($T > 200$ K) assuming the full moment of $9.72\mu_B$ for the free Tb^{3+} ion. The obtained concentrations were found to be in agreement with the nominal concentration within $\sim 4\%$ for all doped samples (horizontal error bars in

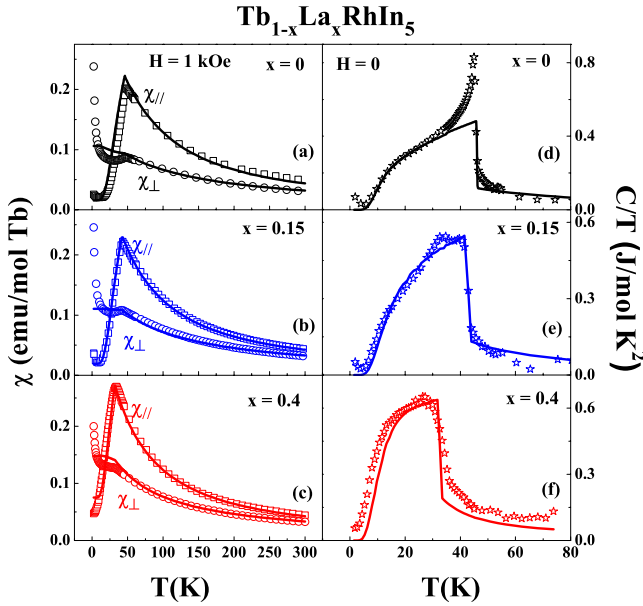


FIG. 2. (Color online) [(a)–(c)] Temperature dependence of the magnetic susceptibility for the applied field of 1 kOe parallel to ab plane (χ_{\perp} and circle symbols) and parallel to the [001] direction (χ_{\parallel} and square symbols) for La concentrations $x=0$ (Ref. 26) 0.15, and 0.40, respectively. [(d)–(f)] Specific heat C/T for $H=0$ applied field. The solid curves for all cases are the best fits to the data using a MF model (Ref. 28).

Fig. 1). Therefore, we have used the nominal concentrations x in this work.

Figure 2 demonstrates the shift to lower values of the temperatures at which the maximum in the susceptibility occurs, and the specific heat has a peak, as the La content increases. These temperatures taken from both measurements coincide reasonably well; therefore, we take this temperature as the Néel temperature T_N for all samples. From this consideration we define T_N for the two doped samples $x=0.15$ and 0.40 as being 43 and 34 K, respectively. The shift of T_N to lower values is a signature from the expected suppression of the long-range-ordered AFM state. For all cases, the susceptibility is anisotropic but the ratio $\chi_{\parallel}/\chi_{\perp}$, defined at the maximum of the χ_{\parallel} data, remains almost the same (roughly 2.12, 2.06, and 1.91 for $x=0, 0.15$, and 0.40, respectively). Additionally, the transitions in the specific-heat data become evidently broader as a function of La doping.

Figure 3 displays the T_N behavior for the studied compounds normalized by the T_N value of the TbRhIn_5 compound ($T_{N,x}/T_{N(x=0)}$) (filled symbols). Similar data obtained for $\text{Ce}_{1-x}\text{La}_x\text{RhIn}_5$ (Ref. 9) (open symbols) are included for comparison. Interestingly, the suppression of T_N as a function of La doping is less dramatic in $\text{Tb}_{1-x}\text{La}_x\text{RhIn}_5$ when compared to $\text{Ce}_{1-x}\text{La}_x\text{RhIn}_5$, and its behavior follows approximately a power-law decrease, which is different from the Ce-based series, where a linear decrease in T_N was observed. The critical concentration for which $T_N \rightarrow 0$ was found to be $x_c \approx 0.70$ for $\text{Tb}_{1-x}\text{La}_x\text{RhIn}_5$ in contrast to the $x_c \approx 0.40$ found for $\text{Ce}_{1-x}\text{La}_x\text{RhIn}_5$.

La-doping perturbations in the AFM state of TbRhIn_5 were further explored through x-ray magnetic diffraction ex-

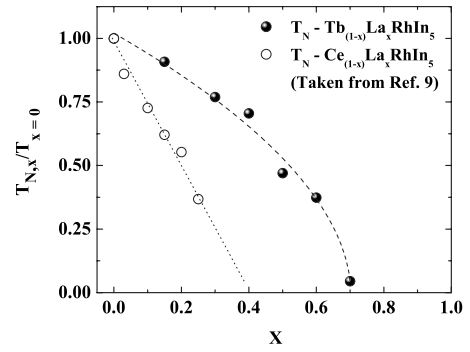


FIG. 3. Normalized Néel temperature T_N ($T_{N,x}/T_{N(x=0)}$) vs x for $\text{Tb}_{1-x}\text{La}_x\text{RhIn}_5$ (filled circles) determined from the specific-heat $C(T)/T$ data. The same data for $\text{Ce}_{1-x}\text{La}_x\text{RhIn}_5$ (Ref. 9) (open circles) are included for comparison. The dotted line represents linear fit to the Ce-based family data while the dashed curve is a power-law fit to the Tb-based data. Extrapolation to $T \rightarrow 0$ for the $\text{Tb}_{1-x}\text{La}_x\text{RhIn}_5$ data gives a critical concentration of about 70%.

periments in a crystal of $\text{Tb}_{0.60}\text{La}_{0.40}\text{RhIn}_5$ from the same batch used for the macroscopic measurements above. These measurements were performed with the incident photon energy at both L_2 and L_3 Tb absorption edges (resonant condition) in order to enhance the small signal from the AFM order of Tb ions below T_N .³³ We found satellite peaks at reciprocal space positions corresponding to the same reciprocal propagation vector found in the nondoped TbRhIn_5 , i.e., $(0\frac{1}{2}\frac{1}{2})$,²⁶ indicating that $\text{Tb}_{0.60}\text{La}_{0.40}\text{RhIn}_5$ orders in a commensurate AFM single- \mathbf{k} structure (\mathbf{k} -propagation vector). Above T_N we only found charge Bragg peaks from the tetragonal HoCoGa_5 -type structure. Other magnetic peaks, representing twinned AFM domains, were also observed at $(\frac{1}{2}0\frac{9}{2})$, $(\frac{1}{2}0\frac{11}{2})$, and $(\frac{1}{2}0\frac{13}{2})$ reciprocal space positions (not shown). A comparison between the intensities of the symmetrically equivalent reflections $(\frac{1}{2}0\frac{9}{2})$ and $(0\frac{1}{2}\frac{9}{2})$ reveals a higher $(0\frac{k}{2}\frac{l}{2})$ domain population over the $(\frac{h}{2}0\frac{l}{2})$ ones (h, k, l integers), with the latter representing roughly 75% of the former.

Open circles in Figs. 4(a) and 4(b) represent the resonance profiles of the superlattice diffraction peak $(0\frac{1}{2}\frac{9}{2})$ around the L_2 (8.253 keV) and L_3 (7.514 keV) Tb absorption edges, respectively, taken at 11 K. The spectral shapes are typical of magnetic scattering from the ordered moments of the Tb ion sublattices, and the peak maxima coincide with the inflection point of the fluorescence spectrum (not shown), revealing the $E1$ electric-dipole-type resonance involving electronic transitions $2p_{1/2} \leftrightarrow 5d$ and $2p_{3/2} \leftrightarrow 5d$. Therefore, we used the energy where maxima in Fig. 4 take place as incident energies for all our measurements of magnetic peaks. Full lines are single-Lorentzian fits from which we were able to get the resonance width as being 8.4 eV for L_2 and 6.7 eV for L_3 . This width is inversely proportional to the resonance core-hole lifetime. The photon energy variation profile at a fixed reciprocal point has proved to be higher [$I(L_{\text{III}})/I(L_{\text{II}}) \approx 3$ eV] and narrower at the L_3 Tb edge, which confirms the L -edge resonances behavior of the Tb^{3+} ion previously suggested in Ref. 34 and observed for other rare-earth-based compounds.^{26,35}

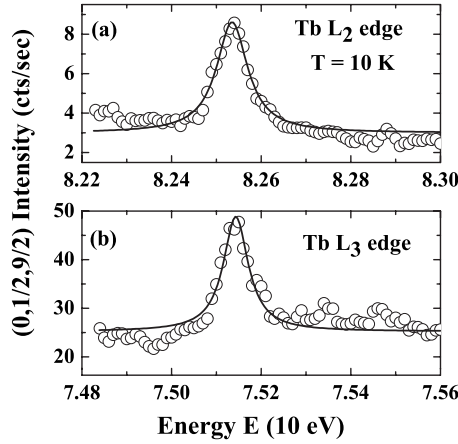


FIG. 4. Energy dependence of the resonant x-ray diffraction signal in $\text{Tb}_{0.60}\text{La}_{0.40}\text{RhIn}_5$ around the $(0\frac{1}{2}\frac{9}{2})$ satellite peak. (a) Data collected around the Tb L_2 absorption edge (8.252 keV) at the base temperature ($T=11$ K). (b) Scattered signal around the Tb L_3 edge (7.514 keV). From a single Lorentzian-profile fit to both data sets (continuous line), we extracted the width of the resonance through the full width at half maximum.

Figure 5 displays the temperature dependence of the $(0\frac{1}{2}\frac{9}{2})$ magnetic Bragg-peak intensities, which is proportional to the Tb magnetization sublattice, obtained from numerical integrations to $\theta-2\theta$ scans (using a pseudo-Voigt function). The data were taken between $T=11$ and -37 K with a T step of 1 K while warming the sample. The inset shows the experimental (filled circles at $T=15$ K and open ones at $T=37$ K) and calculated curves (continuous line) together. Error bars in the main panel represent statistical standard deviation from the fits. The decrease in the Bragg intensities as the temperature is increased toward the bulk T_N denotes also the magnetic character of this reflection. Its smoothness is a signature of a second-order-type transition.

The XRMS results, together with the properties shown in Fig. 2, demonstrate the existence of long-range AFM correlations for the $x=0.40$ doped sample. From the point of view of magnetic diffraction, it seems that the AFM propagation vector does not change as function of La doping up to $x=0.40$. As such, we may argue that the relative spin orientation of neighboring Tb^{3+} ions is not strongly modified by dilution in the $x=0.40$ sample, re-enforcing the long-range character of the RKKY interaction between the Tb^{3+} ions. Further, this result may be indicative that the balance between the Tb first- and second-neighbor interactions (J_1 and J_2 , respectively) is the same as for the nondoped TbRhIn_5 compound.^{24,26}

Nonetheless, from our recent data we cannot determine the direction of magnetic moments in the Tb sublattice through the comparison between observed and calculated integrated intensities of magnetic peaks because only three reflections from the same AFM domains were reached with our experimental setup. Therefore, new data in the resonant condition are required to know the moment orientation for this La-doped sample. Particularly, it should be interesting to include azimuthal dependence of magnetic peak intensity combined with polarization analysis.

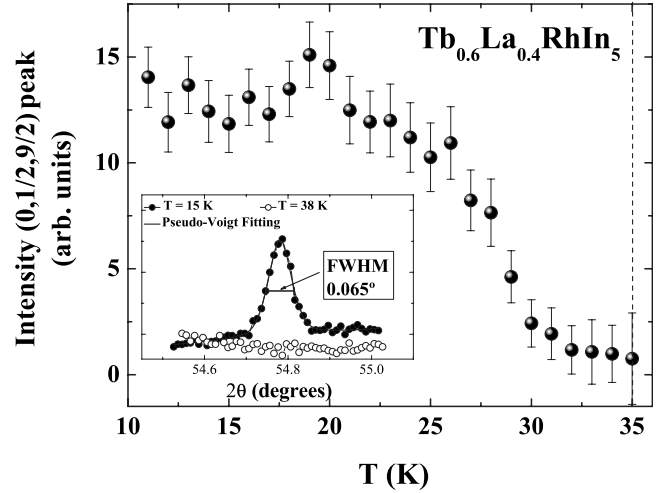


FIG. 5. Temperature dependence of the integrated intensities of the $(0\frac{1}{2}\frac{9}{2})$ magnetic reflection in the temperature range between $T=11$ and 37 K for $\text{Tb}_{0.60}\text{La}_{0.40}\text{RhIn}_5$. The inset shows two longitudinal scans ($\theta-2\theta$) around the $(0\frac{1}{2}\frac{9}{2})$ position: open circles represent the data obtained at $T=15$ K and the filled circles curve was taken at $T=38$ K. Continuous line is a pseudo-Voigt fit to the observed data at $T=15$ K and the vertical dashed line at $T=35$ K shows the Néel temperature, above which no further long-range order can be found.

We now discuss the effects of La doping in the antiferromagnetic interaction between the Tb^{3+} ions in TbRhIn_5 . The first obvious effect is dilution. As La^{3+} replaces Tb^{3+} , the average distance between the remaining Tb^{3+} ions increases and consequently the RKKY magnetic exchange between them decreases. Second, there is the chemical pressure effect induced by the difference in ionic size between La^{3+} and Tb^{3+} . This can affect the CEF effects at the Tb^{3+} site. These effects may be subtle but are not straightforward. Slight modifications in the CEF scheme and/or wave functions can cause significant changes in T_N and in the magnetic anisotropy of the ordered state for low-symmetry systems.²⁸ Lastly, there could exist an effect of chemical disorder caused by a not perfectly homogeneous La distribution through the sample. This may cause competing magnetic interaction between Tb^{3+} ions in different grains, creating multiple spin configuration and/or distribution of T_N , leading to the suppression of the long-range-ordered state.

In order to account for the evolution of the first and second effects above, we have used our MF model from Ref. 28 to fit concomitantly the whole set of data of Fig. 2. In Fig. 6 we show the CEF schemes obtained from the best fits to the data of the representative samples shown in Fig. 2.

Before we proceed with the analysis of the results presented in Fig. 6, it is important to discuss the reliability of these results because CEF parameters obtained from fits to macroscopic measurements data could be mistaken and not unique. It is known that, in general, a given set of parameters can describe very nicely a set of experimental macroscopic results and completely fail in describing others, and that a definitive determination of CEF schemes and/or parameters usually requires direct measurements by inelastic neutron scattering (INS).

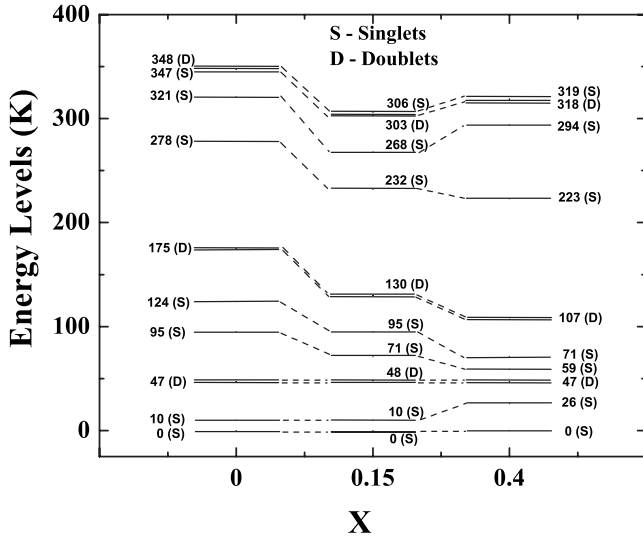


FIG. 6. CEF splitting of the ground-state multiplet of Tb obtained from the simulations of Fig. 2 to $x=0, 0.15,$ and 0.40 using the MF model of Ref. 28.

In an earlier report, we proposed a CEF scheme for pure TbRhIn₅ obtained from fits to magnetic-susceptibility and specific-heat data. This CEF scheme was based on a $\Gamma_5^{(1)}$ doublet ground state and an overall splitting of 310 K.²⁶ Later, low-temperature magnetization experiments³⁶ have shown that this scheme is incompatible with the high-field ($H > 10$ T) magnetization data taken at $T=2$ K for a magnetic field applied along the c axis. As such, in Ref. 36, the authors proposed an alternative scheme of levels with a singlet ground state and overall splitting of about 220 K. This alternative scheme agrees qualitatively with the high-field behavior of their $T=2$ K magnetization data but it does not give a better fit to the $\chi(T)$ and zero-field $C_p(T)$ data unlike that obtained with the CEF scheme of Ref. 26.

Taking into account all the above considerations, we have reanalyzed our $\chi(T)$ and zero-field $C_p(T)$ and the high-field magnetization data of Ref. 36 and obtained CEF scheme of levels present in Fig. 6 for pure TbRhIn₅. The CEF scheme has a singlet ground state with a first excited singlet at 10 K and an overall splitting of ~ 350 K (see Fig. 6, left scheme). Although both present a singlet ground state, the TbRhIn₅ CEF scheme of Fig. 6 and the one from Ref. 36 display appreciable differences in terms of energy level and wave functions. This level of controversy usually requires direct measurements by INS to be completely solved; however, our preliminary CEF parameters determination and data fits proceeding allow us to follow the La-doping-induced changes in the crystal field and the modifications on the AFM state of

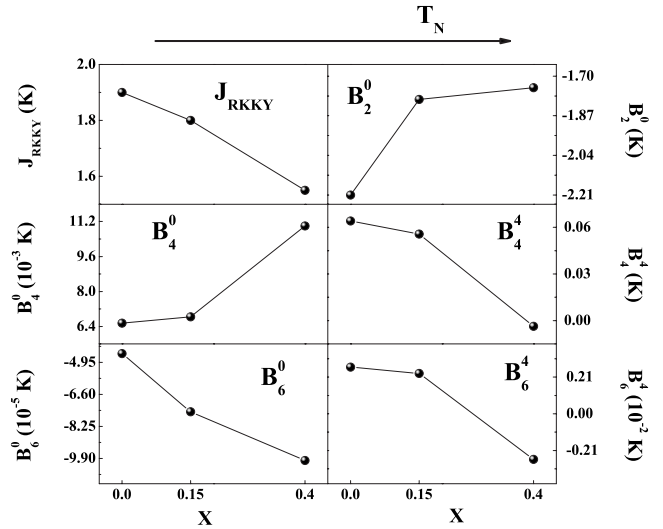


FIG. 7. CEF parameters evolution as the La concentration is increased.

TbRhIn₅. Further, it is important to emphasize that the qualitative evolution of the CEF scheme and parameters as a function of La doping was found to be nearly independent of the details of a particular choice of CEF parameters (and scheme) for pure TbRhIn₅ (Fig. 6 or Ref. 36).

Analyzing the La-doping evolution of the CEF energy-level schemes in Fig. 6, we observe that for $x \leq 0.40$ the best fits yield ground-state singlets and a nonmonotonic evolution of the overall CEF splitting as a function of La doping. However, one can clearly observe a trend in the low- T energy levels ($T < 200$ K), showing a compression to lower-temperature ranges. This effect causes the increase in the low- T magnetic entropy and may certainly affect T_N and the ordered state.²⁸ Additionally, the set of CEF parameters giving place to the fits of Fig. 2, and to the schemes of Fig. 6, shows systematic changes as the La concentration is increased (see Table I and Fig. 7).

From Fig. 7 one can notice the effect of dilution by decreasing the effective Tb³⁺-Tb³⁺ exchange interaction J_{RKKY} as well as the modification of the crystal-field parameters due to the lattice expansion caused by La doping. Although these two effects may be expected, it is not obvious how they are combined to suppress T_N and to affect the details of the ordered state of complex magnetic systems in dilution studies.

In order to explore separately the two effects above, we used our MF model to simulate the evolution of T_N while changing the CEF parameters values of Table I for a fixed $J_{RKKY}=0.2$ meV (obtained for the nondoped TbRhIn₅). Alternatively, we study the T_N suppression with the La doping

TABLE I. T_N and CEF parameters for Tb_{1-x}La_xRhIn₅.

	T_N (K)	J_{R-R} (K)	B_{20} (K)	B_{40} (K)	B_{44} (K)	B_{60} (K)	B_{64} (K)
TbRhIn ₅	45.6	1.9	-2.2	6.6×10^{-3}	6.4×10^{-2}	-4.5×10^{-5}	2.7×10^{-3}
Tb _{0.85} La _{0.15} RhIn ₅	42.8	1.8	-1.8	6.8×10^{-3}	5.6×10^{-2}	-7.5×10^{-5}	2.3×10^{-3}
Tb _{0.60} La _{0.40} RhIn ₅	32.0	1.6	-1.8	1.1×10^{-2}	-3.6×10^{-3}	-1.0×10^{-4}	-2.6×10^{-3}

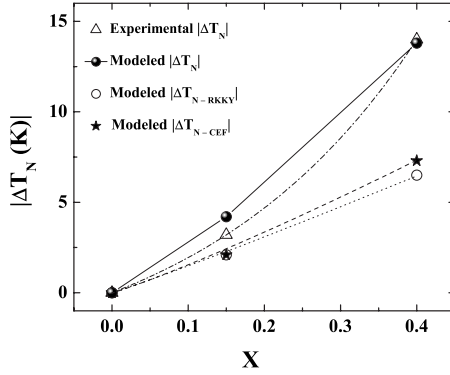


FIG. 8. Néel temperature variation $|\Delta T_N|$ as a function of La content while changing CEF parameters and J_{RKKY} is fixed to 0.2 meV ($|\Delta T_{N-CEF}|$, star symbols) and as J_{RKKY} was changed with CEF parameters fixed ($|\Delta T_{N-RKKY}|$, open circle symbols). Modeled $|\Delta T_N|$ is the result of considering both effects together.

solely due to the decrease in J_{RKKY} and keeping unchanged the CEF scheme of the $TbRhIn_5$ compound. The results of these procedures can be seen in Fig. 8. From this plot it is evident that the CEF changes and the decrease in J_{RKKY} have comparable effects on the T_N suppression. The T_N shift due to the changes of the CEF parameters by La doping, $|\Delta T_{N-CEF}|$, is nearly the same as the T_N shift resulting from the increase in the Tb^{3+} - Tb^{3+} average distance changes by dilution, $|\Delta T_{N-RKKY}|$. However, both effects had to be taken into account to best reproduce the data of Fig. 2 and the experimental T_N suppression of Fig. 8 (which we called modeled $|\Delta T_N|$). The significant decrease in T_N induced by CEF is a nontrivial and important result that indicates that the effects of CEF changes should be generally taken into account when important temperature scales are mapped and analyzed as function of doping in the $RRhIn_5$ family and related compounds.²⁻¹⁷

Another important aspect of our results for $Tb_{1-x}La_xRhIn_5$ is the role of disorder on the properties of this series. On one hand, our theoretical model does not include any kind of disorder (for instance, a random distribution of T_N and/or CEF parameters). On the other hand, our electrical resistivity data (not shown) for all the studied samples show no evolution of the residual resistivity ρ_0 with the La content and lies in the range between ~ 3.5 and $10 \mu\Omega$ cm, which are typical values for ordered intermetallic compounds. This indicates that the disorder present in our samples does not strongly affect the electronic scattering mechanism as a function of La content. Therefore, we can conclude that chemical defects such as dislocations, impurities, grain boundaries, random antisite disorder, and strain are not present in our samples.

However, the specific-heat and magnetic-susceptibility data for the $Tb_{1-x}La_xRhIn_5$ compounds with long-range magnetic AFM order show remarkably broad transitions at T_N if compared to the nondoped $TbRhIn_5$ compound, which makes the presence of disorder evident and leads to the failure of our model to simulate the data for samples with higher La concentration. Thus, this disorder should be mainly in terms of a T_N distribution caused a distribution of J_{RKKY} and CEF parameters rather than chemical disorder. One should notice that Tb 4f electrons are highly localized and the contribution

of the magnetic scattering in the electrical resistivity is much smaller than in the case of heavy fermions.

The broadening in the specific-heat data has been also observed and discussed in Ref. 11 within the $Ce_{1-x}La_xRhIn_5$ series, where they have shown that the anisotropic short-range order taking place in $Ce_{0.50}La_{0.50}RhIn_5$ compound induces in-plane magnetic disorder and broadens the profile of the specific-heat data. This was also earlier demonstrated by McCoy and Wu in Ref. 37. Therefore, for the La-doped Tb -based series of this work, we claim that distribution of J_{RKKY} and CEF parameters should be the origin of the observed T_N distribution in our specific-heat data. Nonetheless, whether this magnetic disorder manifests itself as dropletlike short-range order near T_N or by multiple magnetic modulated wave vectors coexisting with the long-range order remains and it has to be investigated by future XRMS experiments with higher-energy and -temperature resolutions. On the other hand, it is interesting to notice that we do not see a clear contribution of this magnetic disorder in the suppression of the average T_N for $x \leq 0.40$, as we were able to simulate T_N decreasing only by considering dilution and CEF tuning effects (see Figs. 2 and 8).

Finally, the last interesting point to be addressed is the comparison between the T_N suppression in $Tb_{1-x}La_xRhIn_5$ and in its heavy fermions counterpart $Ce_{1-x}La_xRhIn_5$ given in Fig. 3. It is evident that the critical concentration $x_c \approx 0.70$ for $Tb_{1-x}La_xRhIn_5$ is much higher than the $x_c \approx 0.40$ found for $Ce_{1-x}La_xRhIn_5$.⁹ While $x_c \approx 0.40$ for $Ce_{1-x}La_xRhIn_5$ is close to the 2D percolation threshold for a Heisenberg square lattice,^{9,18} $x_c \approx 0.70$ for $Tb_{1-x}La_xRhIn_5$ is the same as for a three-dimensional (3D) lattice. Thus, a simple argument to understand the increase in x_c for $Tb_{1-x}La_xRhIn_5$ may be given by its more 3D character, as the tetragonal lattice parameters ratio c/a decreases along the $RRhIn_5$ series.^{22,26} On the other hand, it is clear that the nonlinear suppression of T_N is in obvious contrast to the linear behavior found for $Ce_{1-x}La_xRhIn_5$ and even for cubic $Ce_{1-x}La_xIn_3$ ($x_c \approx 0.65$). In this regard, it is worth noting that for $Tb_{1-x}La_xRhIn_5$ we found a roughly linear decrease in T_N as a function of x up to $x \sim 0.40$ (see Fig. 3). This linear behavior of the T_N decrease could be successfully understood by the monotonic evolution of J_{RKKY} and the CEF parameters as a function of x (see Figs. 7 and 8). However, for $0.40 < x \leq 0.70$, the T_N decrease becomes more abrupt and, as stated in the previous paragraph, we were no longer able to fit the data using our model in this range of concentration, presumably due to the role of disorder in the specific-heat data. Therefore, we speculate that the nontrivial T_N suppression for $0.40 < x \leq 0.70$ in $Tb_{1-x}La_xRhIn_5$ may be related to the details of the disorder effects near the dilution limit. This effect has not been observed in $Ce_{1-x}La_xRhIn_5$ and cubic $Ce_{1-x}La_xIn_3$ because the difference in ionic size between Tb^{3+} and La^{3+} ions is much larger than between Ce^{3+} and La^{3+} , and for the latter case one has also to consider the possible important role of doping effect on the 4f-conduction electrons hybridization and Kondo compensation, which are not present in Tb -based compounds. In addition, the percolation problem including an exchange interaction with long-range character, as the RKKY interaction, has not been completely understood even in a perfectly ordered system.³⁸ In

fact, our XRMS results for $x=0.40$ indicate that the relative exchange interaction between neighboring Tb^{3+} ions is very robust against La doping which suggests that, due to the long-range character of the RKKY interaction, the dilution-induced J_{RKKY} decrease may be much smaller than that expected for a Heisenberg square lattice,^{9,18} especially for a more 3D system.

IV. CONCLUSIONS

In summary, we have performed magnetic-susceptibility and specific-heat measurements for the $\text{Tb}_{1-x}\text{La}_x\text{RhIn}_5$ ($0.15 \leq x < 0.90$) diluted compounds. Particularly, we discussed the results from representative samples with La concentrations $x=0.15$ and 0.40 and compared with previous results from the nondoped TbRhIn_5 . We also presented preliminary results of resonant x-ray magnetic scattering experiments in $\text{Tb}_{0.60}\text{La}_{0.40}\text{RhIn}_5$. The AFM structure revealed is commensurate with the same propagation vector ($0\frac{1}{2}\frac{1}{2}$) of the nondoped compound, which indicates the same relative in-

teraction J_1/J_2 between Tb^{3+} neighbors. Néel temperature decreases with a nonlinear behavior as a function of lanthanum concentration and extrapolates to zero at roughly 70% of La content, which demonstrates that for TbRhIn_5 the non-magnetic La substitution shifts the dilution limit differently to $x_c \sim 40\%$ observed for $\text{Ce}_{1-x}\text{La}_x\text{RhIn}_5$ and $(\text{Ce}_{1-x}\text{La}_x)_2\text{RhIn}_8$ families. Furthermore, our mean-field model simulation for $\text{Tb}_{1-x}\text{La}_x\text{RhIn}_5$ ($x \leq 0.40$) reveals that the crystal-field scheme evolves as a function of doping and that this evolution affects T_N as much as the decrease in J_{RKKY} due to dilution. This effect may be of great importance in phase diagrams of complex magnetic systems where the AFM is tuned to zero temperature by chemical substitution.

ACKNOWLEDGMENTS

This work was supported by FAPESP (SP-Brazil) Grants No. 06/50511-8, No. 06/60440-0, and No. 06/60387-2; CNPq (Brazil) Grant No. 305161/2006-7; and Capes (Brazil) Grant No. 065/2007. LNLS is also acknowledged for beamtime at XRD2 beamline.

-
- ¹M. A. Continentino, Braz. J. Phys. **35**, 197 (2005); A. Schroeder, G. Aeppli, P. Coleman, R. Ramazashvili, R. Coldea, M. Adams, E. Bucher, D. F. McMorrow, H. V. Lohneysen, and O. Stockert, Int. J. Mod. Phys. B **16**, 3031 (2002).
- ²P. G. Pagliuso, C. Petrovic, R. Movshovich, D. Hall, M. F. Hundley, J. L. Sarrao, J. D. Thompson, and Z. Fisk, Phys. Rev. B **64**, 100503(R) (2001).
- ³P. G. Pagliuso, R. Movshovich, A. D. Bianchi, M. Nicklas, N. O. Moreno, J. D. Thompson, M. F. Hundley, J. L. Sarrao, and Z. Fisk, Physica B **312-313**, 129 (2002).
- ⁴L. D. Pham, Tuson Park, S. Maquilon, J. D. Thompson, and Z. Fisk, Phys. Rev. Lett. **97**, 056404 (2006).
- ⁵E. N. Hering, H. A. Borges, S. M. Ramos, M. B. Fontes, E. Baggio-Saitovich, E. M. Bittar, L. Mendonça Ferreira, R. Lora-Serrano, C. Adriano, P. G. Pagliuso, J. L. Sarrao, and J. D. Thompson, Physica B **403**, 780 (2008).
- ⁶E. D. Bauer, C. Capan, F. Ronning, R. Movshovich, J. D. Thompson, and J. L. Sarrao, Phys. Rev. Lett. **94**, 047001 (2005).
- ⁷V. S. Zapf, E. J. Freeman, E. D. Bauer, J. Petricka, C. Sirvent, N. A. Frederick, R. P. Dickey, and M. B. Maple, Phys. Rev. B **65**, 014506 (2001).
- ⁸N. O. Moreno, M. F. Hundley, P. G. Pagliuso, R. Movshovich, M. Nicklas, J. D. Thompson, J. L. Sarrao, and Z. Fisk, Physica B **312-313**, 274 (2002).
- ⁹P. G. Pagliuso, N. O. Moreno, N. J. Curro, J. D. Thompson, M. F. Hundley, J. L. Sarrao, Z. Fisk, A. D. Christianson, A. H. Lacerda, and A. L. Cornelius, Phys. Rev. B **66**, 054433 (2002).
- ¹⁰V. F. Correa, L. Tung, S. M. Hollen, P. G. Pagliuso, N. O. Moreno, J. C. Lashley, J. L. Sarrao, and A. H. Lacerda, Phys. Rev. B **69**, 174424 (2004).
- ¹¹B. E. Light, Ravhi S. Kumar, A. L. Cornelius, P. G. Pagliuso, and J. L. Sarrao, Phys. Rev. B **69**, 024419 (2004).
- ¹²U. Alver *et al.*, Phys. Rev. B **64**, 180402(R) (2001).
- ¹³A. D. Christianson, E. D. Bauer, P. G. Pagliuso, N. O. Moreno, M. F. Hundley, and J. L. Sarrao, Physica B **312-313**, 241 (2002).
- ¹⁴W. Bao, A. D. Christianson, P. G. Pagliuso, J. L. Sarrao, J. D. Thompson, A. H. Lacerda, and J. W. Lynn, Physica B **312-313**, 120 (2002).
- ¹⁵M. A. Tanatar *et al.*, Phys. Rev. Lett. **95**, 067002 (2005).
- ¹⁶C. Petrovic, S. L. Budko, V. G. Kogan, and P. C. Canfield, Phys. Rev. B **66**, 054534 (2002).
- ¹⁷S. Nakatsuji, S. Yeo, L. Balicas, Z. Fisk, P. Schlottmann, P. G. Pagliuso, N. O. Moreno, J. L. Sarrao, and J. D. Thompson, Phys. Rev. Lett. **89**, 106402 (2002).
- ¹⁸K. Kato, S. Todo, K. Harada, N. Kawashima, S. Miyashita, and H. Takayama, Phys. Rev. Lett. **84**, 4204 (2000).
- ¹⁹Johnpierre Paglione, T. A. Sayles, P.-C. Ho, J. R. Jeffries, and M. B. Maple, Nat. Phys. **3**, 703 (2007).
- ²⁰L. Mendonça Ferreira, T. Park, V. Sidorov, M. Nicklas, E. M. Bittar, R. Lora-Serrano, E. N. Hering, S. M. Ramos, M. B. Fontes, E. Baggio-Saitovich, H. Lee, J. L. Sarrao, J. D. Thompson, and P. G. Pagliuso, Phys. Rev. Lett. **101**, 017005 (2008).
- ²¹P. G. Pagliuso, J. D. Thompson, M. F. Hundley, and J. L. Sarrao, Phys. Rev. B **62**, 12266 (2000).
- ²²P. G. Pagliuso, J. D. Thompson, M. F. Hundley, J. L. Sarrao, and Z. Fisk, Phys. Rev. B **63**, 054426 (2001).
- ²³E. Granado, P. G. Pagliuso, C. Giles, R. Lora-Serrano, F. Yokaichiya, and J. L. Sarrao, Phys. Rev. B **69**, 144411 (2004).
- ²⁴E. Granado, B. Uchoa, A. Malachias, R. Lora-Serrano, P. G. Pagliuso, and H. Westfahl, Phys. Rev. B **74**, 214428 (2006).
- ²⁵R. Lora-Serrano, L. Mendonça Ferreira, D. J. Garcia, E. Miranda, C. Giles, J. G. S. Duque, E. Granado, and P. G. Pagliuso, Physica B **384**, 326 (2006).
- ²⁶R. Lora-Serrano, C. Giles, E. Granado, D. J. Garcia, E. Miranda, O. Aguero, L. Mendonça Ferreira, J. G. S. Duque, and P. G. Pagliuso, Phys. Rev. B **74**, 214404 (2006).
- ²⁷C. Adriano, R. Lora-Serrano, C. Giles, F. de Bergevin, J. C.

- Lang, G. Srajer, C. Mazzoli, L. Paolasini, and P. G. Pagliuso, *Phys. Rev. B* **76**, 104515 (2007).
- ²⁸P. G. Pagliuso *et al.*, *J. Appl. Phys.* **99**, 08P703 (2006).
- ²⁹S. Chang, P. G. Pagliuso, W. Bao, J. S. Gardner, I. P. Swainson, J. L. Sarrao, and H. Nakotte, *Phys. Rev. B* **66**, 132417 (2002).
- ³⁰Z. Fisk and J. P. Remeika, in *Handbook on the Physics and Chemistry of Rare Earths*, edited by K. A. Gschneidner, Jr. and L. Eying (Elsevier, Amsterdam, 1989), Vol. 12, p. 53.
- ³¹A. Malachias, E. Granado, R. Lora-Serrano, P. G. Pagliuso, and C. A. Perez, *Phys. Rev. B* **77**, 094425 (2008).
- ³²T. J. B. Holland and S. A. T. Redfern, *Miner. Mag.* **61**, 65 (1997).
- ³³M. Blume, *J. Appl. Phys.* **57**, 3615 (1985).
- ³⁴M. van Veenendaal, J. B. Goedkoop, and B. T. Thole, *Phys. Rev. Lett.* **78**, 1162 (1997).
- ³⁵J. W. Kim, Y. Lee, D. Wermeille, B. Sieve, L. Tan, S. L. Bud'ko, S. Law, P. C. Canfield, B. N. Harmon, and A. I. Goldman, *Phys. Rev. B* **72**, 064403 (2005).
- ³⁶N. V. Hieu *et al.*, *J. Phys. Soc. Jpn.* **76**, 064702 (2007).
- ³⁷B. M. McCoy and T. T. Wu, *Two-Dimensional Ising Model* (Harvard University Press, Cambridge, 1973).
- ³⁸T. Vojta and J. A. Hoyos, in *Proceedings of the 14th International Conference on Recent Progress in Many-Body Theories*, edited by J. Boronat, G. Astrakharchik, and F. Mazzanti (World Scientific, Barcelona, Spain, 2007), p. 235; J. A. Hoyos and Thomas Vojta, *Phys. Rev. B* **74**, 140401(R) (2006).